



The role of pulse sequences in controlling ultrafast intramolecular dynamics with four-wave mixing

VADIM V. LOZOVY[†], IGOR PASTIRK[‡], EMILY J. BROWN,
BRUNA I. GRIMBERG and MARCOS DANTUS[§]

Department of Chemistry and Center for Fundamental Materials Research,
Michigan State University, East Lansing, MI 48824, USA

This article seeks to provide a fundamental understanding of time-resolved four-wave mixing (FWM) processes based on a large body of experimental measurements on a model system consisting of isolated iodine molecules. The theoretical understanding is based primarily on a diagrammatic approach. Double-sided Feynman diagrams are used to classify and describe the coherent FWM processes involved in the signal obtained with each pulse sequence. Different pulse sequences of degenerate femtosecond pulses are shown to control the optical phenomena observed, that is transient grating, reverse-transient grating, photon echo and virtual photon echo. The experimental data reveal clear differences between the nonlinear optical phenomena. We find that the virtual photon echo sequence $k_1 - k_2 + k_3$ is the most efficient for controlling the observation of ground- or excited-state dynamics. The strategy followed to make this assessment was to compare transients when the time delay between two of the three pulses set in or out of phase with the excited-state vibrational dynamics. We have obtained a signal from pulse sequences $k_1 + k_2 - k_3$ for which FWM signal generation for this two-electronic-level system is forbidden. This signal can be explained by the cascading of a first-order polarization and a second-order process to generate the FWM signal. The implications of our findings are discussed in the context of multiple-pulse methods for the control of intramolecular dynamics.

1. Introduction

This article explores the different four-wave mixing (FWM) phenomena that can be obtained as a function of pulse sequences using degenerate ultrafast pulses. The goal is to reach a more fundamental understanding of these processes by learning how the time order between the pulses can be used to control the different nonlinear optical responses that lead to signal formation. The data from this systematic approach provide the relative intensities from the different nonlinear processes and reveal pulse sequences that are amenable to control electronic state excitation. The experimental data obtained for different pulse sequences directly demonstrate the need to separate bra and ket interactions for a complete understanding of FWM experiments with non-collinear laser pulses. We have found that under certain conditions, for example gas-phase samples and high sample concentrations, a cascading process can occur whereby the free-induction decay emission (FIDE) stimulated by one of the pulses can mix with two other beams to produce an additional source of signal, namely cascade-free-induction decay–four-wave mixing (C–FID–FWM). This article provides a large body

[†] Permanent address: N.N. Semenov Institute of Chemical Physics, Russian Academy of Sciences, Moscow, Russia.

[‡] Affiliated with the Institute for Nuclear Sciences ‘VINCA’, Belgrade, Yugoslavia.

[§] Author for correspondence. E-mail: dantus@msu.edu

of experimental data on a model system consisting of isolated molecular iodine, which is well understood and can be used to refine present theories on FWM.

Nonlinear optical methods, such as FWM, have been used to investigate solids, liquids and gases almost since the invention of the laser (see for example [1–9]). These nonlinear optical techniques are well known [10–24], and many texts have been written on these subjects [25–28]. In the condensed phase, the collective polarizability of the sample contributes to the nonlinear response and it is difficult to separate the intermolecular from the intramolecular processes that cause the observed signal. In dilute gases, it is much easier to analyse in detail the photophysical processes that lead to signal formation. Inhomogeneous broadening is small and the coherence decay is much longer than the laser pulse duration. This latter characteristic leads to long-lived signals, of the order of 100 ps, which in turn allow for very accurate analysis.

Gas-phase FWM studies have a long history, starting probably with the observation of photon echoes (PEs) in SF₆ [2] and the first observation of molecular rotation by a third-order nonlinear process [4]. Numerous gas-phase applications of transient grating techniques were pioneered by Fayer and co-workers [7, 29, 30], especially for the study of flames. These novel probes have been applied to the study of femtosecond dynamics in the gas phase [31–40]. Zewail and co-workers [34] used degenerate four-wave mixing (DFWM) for probing reaction dynamics. Materny and co-workers [35–39] have studied iodine vapour using time-resolved coherent anti-Stokes Raman scattering (CARS) and DFWM. By varying the time delay of one of the incident pulses while maintaining the other two incident pulses overlapped in time, they showed that vibrational and rotational dynamics can be observed for both the ground and excited electronic states. Knopp *et al.* [41] have used two-dimensional time-delay CARS to study high-energy ground-state vibrations.

Brown *et al.* [42] used off-resonance transient grating (TG) methods to study the response of atoms as well as polyatomic molecules in the gas phase and derived a semiclassical expression to analyse the rotational coherences observed in the data. Resonance TG measurements confirmed the observation of ground and excited states [42]. Dantus and co-workers [43, 44] have explored different laser pulse sequences in three-pulse FWM to control the observation of ground- or excited-state dynamics. Dantus and co-workers [45, 46] have also shown that the spectrally dispersed three-pulse FWM method adds an important dimension to the study of nonlinear phenomena with transform limited and chirped pulses.

Gas-phase molecular iodine was chosen for this study for various reasons.

- (i) The visible $X^1\Sigma_{0+g} \leftrightarrow B^3\Pi_{0+u}$ transition has been well characterized by frequency- [47, 48] and time-domain spectroscopies [43, 45, 46, 49]
- (ii) The vibrational periods of both the X and the B states are longer than the duration of our laser pulses, allowing us to excite wave packets impulsively in each electronic state.
- (iii) The vibrational periods of the X and B states are quite different, 160 and 307 fs respectively, making the assignment of the signal relatively easy.
- (iv) At the wavelength of excitation, molecular iodine can be treated as a two-(electronic)-level system. The state reached by two-photon excitation is repulsive and does not contribute to the signal discussed in this study.

This article is organized as follows. In section 2 we present a brief theoretical description of FWM based on a density matrix formulation. We describe a diagrammatic approach to identify the third-order processes that contribute to a

particular FWM phenomenon. We also apply wave packet calculations to understand some aspects of the observed signal. In section 3 we describe the experimental set-up for the present measurements. In section 4 we present experimental results for all the different pulse sequences and we discuss some of the main observations. In section 5, we conclude on the major observations of the study and their implications regarding FWM methods for characterizing and controlling intramolecular dynamics.

2. Theory

There are numerous publications in the literature on the nature of nonlinear optical processes (see for example [25–27]). Some works involve the density matrix approach, whereas in other cases the wave packet formalism is used to understand FWM-type processes [50, 51]. We find that the density matrix approach provides a complete framework for interpreting nonlinear optic phenomena [25–27, 43, 52]. The density matrix approach naturally incorporates all the vibrational and rotational states initially populated necessary to express the collective nature of a coherent process.

Three-pulse FWM involves a sequential interaction of three electric fields with a molecular ensemble. The incident pulses are typically arranged in the forward-box geometry shown in figure 1 (*a*), and the coherent signal is emitted in the direction \mathbf{k}_s with frequency ω_s . Both the wave-vector and the frequency of the signal are linear combinations of the wave-vectors and frequencies of the applied fields. The wave-vector $\mathbf{k}_s = \mathbf{k}_a - \mathbf{k}_b + \mathbf{k}_c$ satisfies the phase-matching condition, ensuring conservation of energy and momentum. The source of the signal is the third-order polarization $P_s^{(3)}(t)$ in the direction \mathbf{k}_s that arises after weak interactions with the applied fields. For homodyne detection, the intensity of the signal is [25, 26]

$$I_{\text{FWM}} \propto \int_{-\infty}^{\infty} \left| P_s^{(3)}(t) \right|^2 dt \quad (1)$$

When the applied electric fields are short laser pulses, various rotational, vibrational and, in some cases, electronic levels can be excited impulsively. In those cases the signal reflects the coherent superposition of molecular polarizations, showing coherent oscillations (or quantum beats). In this way, the optical polarization contains information regarding the electronic and nuclear dynamics manifested in the spectra. The coherent signals in a FWM process involve the entire molecular ensemble that is interrogated by the laser electric fields. The interpretation of the signals requires the density matrix formalism for which the statistical nature of the quantum mechanical ensemble is explicitly taken into account. The third-order polarization of the molecular ensemble is defined as [25, 27]

$$P_s^{(3)}(t) = \text{Tr}[\hat{P}\hat{\rho}_s^{(3)}(t)], \quad (2)$$

where \hat{P} is the polarization operator and $\hat{\rho}_s^{(3)}(t)$ is the third-order density matrix with a spatial dependence $\mathbf{k}_s \cdot \mathbf{r}$.

The temporal evolution of the density matrix can be represented diagrammatically [25–27, 53–56] by double-sided Feynman diagrams (DSFDs) [25, 26, 57] or ladder diagrams [58]. Each diagram is associated with a sequence of transformations or pathway in a phase space of the density matrix. The total number of diagrams for a given direction \mathbf{k}_s is 48 [25–27]. However, under the rotating-wave approximation (RWA), the number of possible pathways is reduced to eight. When the system includes only two electronic states, the frequency dependence of the slowly rotating

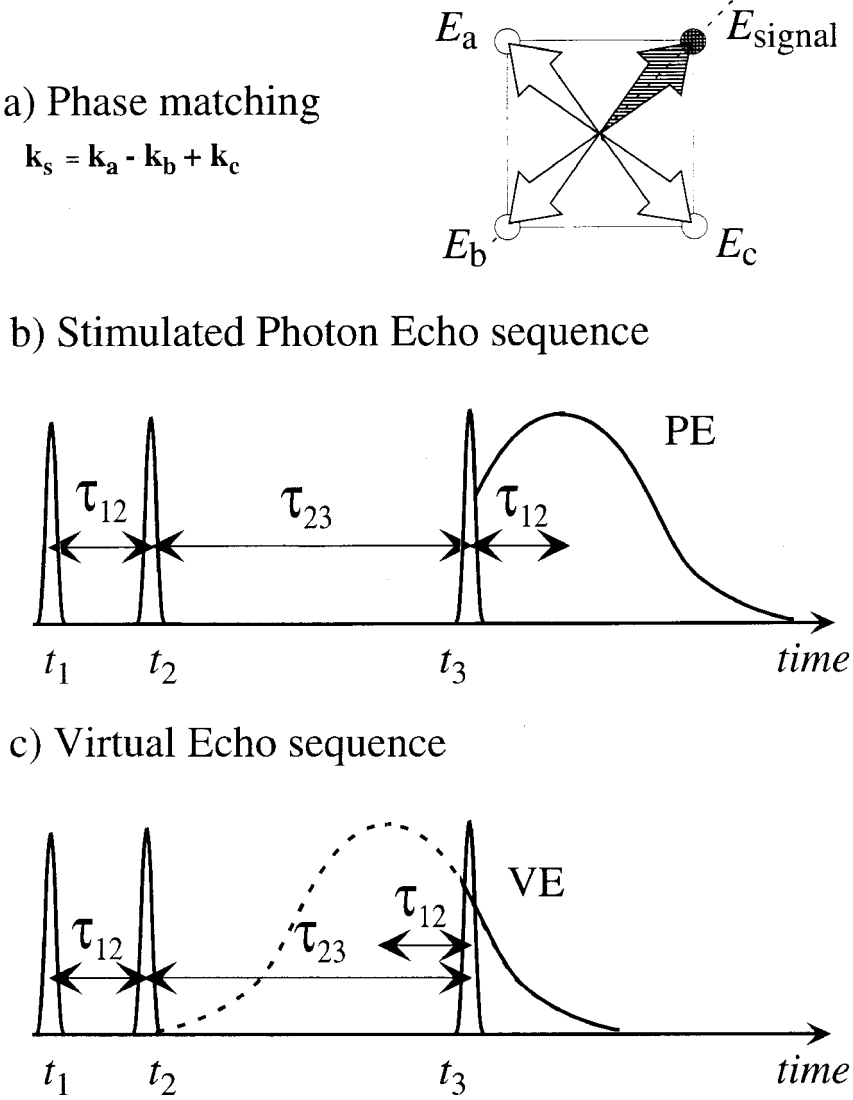


Figure 1. (a) Beam arrangement in the forward-box configuration for the three-pulse FWM experiment. The three laser fields are applied in a given temporal sequence and overlapped spatially in the sample. The signal is detected in the direction of the wave-vector \mathbf{k}_s that satisfies the phase-matching condition. The broken curve indicates a plane of symmetry that makes fields E_a and E_c equivalent. (b) Temporal sequence of the three laser pulses for a virtual echo (VE) measurement. τ_{12} and τ_{23} are the time delays between first and second pulses and between second and third pulses respectively. (c) Temporal sequence of the three laser pulses for a VE measurement. Note that the rephasing occurs at a time $t_3 + (t_2 - t_1)$ for the stimulated PE signal and $t_3 - (t_2 - t_1)$ for the VE signal.

terms is $\exp [i(\omega - \omega_{eg})t]$, where ω is the carrier frequency of the pulses resonant with the transition frequency ω_{eg} . Based on the RWA the contribution of slowly rotating terms is much greater; therefore pulse sequences having the first two electric fields interact with opposite wave-vectors are primarily responsible for the FWM signal. As a consequence, the first two pulses of a three-pulse FWM sequence form gratings in the

direction $\pm(\mathbf{k}_1 - \mathbf{k}_2)$; the third pulse Bragg diffracts from that grating and the direction of the signal is given by $\mathbf{k}_s = \mathbf{k}_3 \pm (\mathbf{k}_1 - \mathbf{k}_2)$. The specific pulse sequence, indicated by the subscripts 1, 2 and 3, determines a specific nonlinear process detected at the direction \mathbf{k}_s and the corresponding coherent transient effect probed.

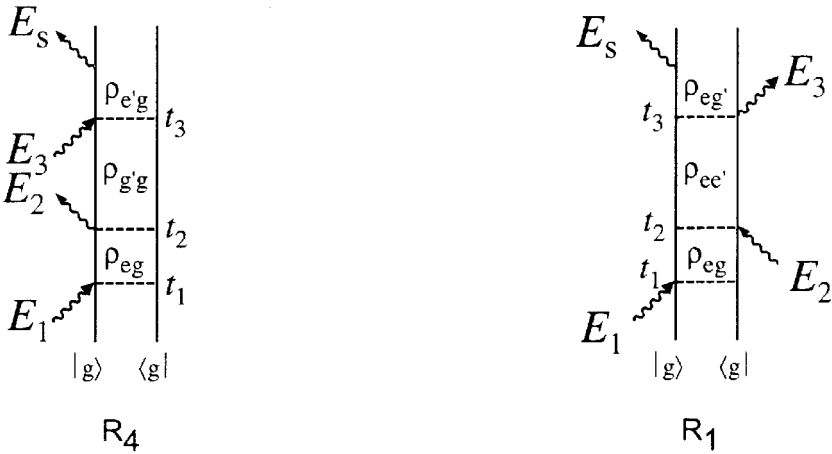
When the signal is collected at $\mathbf{k}_s = -\mathbf{k}_1 + \mathbf{k}_2 + \mathbf{k}_3$, the signal corresponds to a stimulated PE process [27]. When the signal is collected at $\mathbf{k}_s = \mathbf{k}_1 - \mathbf{k}_2 + \mathbf{k}_3$, the signal has been called a virtual photon echo (VE) phenomenon [59, 60]. Alternative names for this non-rephasing FWM signal can be found in the literature [27, 61, 62]. One of the key differences between VE and PE phenomena is the fact that PE phenomena can be regarded as a reversible decay process for which the polarization rephases after the interaction with the third laser pulse [1, 2, 25–27, 63]. For PE this polarization reaches a maximum at a time $t_3 + (t_2 - t_1)$ (see figure 1(b)) whereas for VE the polarization reaches a maximum at a time $t_3 - (t_2 - t_1)$ (see figure 1(c)); hence we have the name virtual and the lack of observable rephasing [25–27, 63]. This difference is of critical importance for samples where the inhomogeneous broadening is significant, such as in liquids and solids. For PE measurements, the inhomogeneous dephasing is cancelled by the optical rephasing. These effects are sufficiently noticeable in gas-phase samples as demonstrated below.

Each experimental signal obtained with a specific pulse sequence in the direction \mathbf{k}_s is the coherent sum of the signal corresponding to several third-order pathways in the Liouville space (as shown later in figures 3, 4 and 6–8). Therefore, more than one diagram may be associated with a particular three-pulse FWM phenomenon. Each diagram contributes additively to the overall third-order polarization and the signal is proportional to the square of that polarization. Diagrams for which the first interaction is on the ket side correspond to VE phenomena, whereas the diagrams that initially show a bra side interaction correspond to PE phenomena.

We have chosen the pulse sequence $\mathbf{k}_1 - \mathbf{k}_2 + \mathbf{k}_3$ (figure 2) to demonstrate the different density matrix pathways involved in a VE process. In the DSFD (figure 2(a)), the bra (right-hand side vertical line) and the ket (left-hand side vertical line) interactions are kept separately. Each electric field interaction is indicated with a short slanted arrow. The convention for the sign of the electric field wave-vectors is that positive wave-vectors with $\exp[i(\mathbf{k} \cdot \mathbf{r} - \omega t)]$ point to the right while negative wave-vectors with $\exp[-i(\mathbf{k} \cdot \mathbf{r} - \omega t)]$ point to the left on the diagram. Its relative position and label t_1 , t_2 or t_3 are used to indicate the time ordering of the laser pulse in a given sequence. The first interaction with the system causes a change on only one side of the Feynman diagram (bra or ket), giving rise to an electronic coherence, designated $\rho_{eg}^{(1)}$ or $\rho_{eg}^{(1)}$ respectively. The second interaction produces a population change, designated $\rho_{gg}^{(2)}$ or $\rho_{ee}^{(2)}$, and a ro-vibrational coupling within each electronic state, designated $\rho_{gg'}^{(2)}$ or $\rho_{gg'}^{(2)}$ in the ground state or $\rho_{ee'}^{(2)}$ or $\rho_{ee'}^{(2)}$ in the excited state. The symbols gg' and ee' represent different ro-vibrational levels in the ground and excited states respectively. Note that the DSFD on the left, labelled R_4 , proceeds through the formation of $\rho_{gg'}^{(2)}$ while the DSFD on the right, labelled R_1 , proceeds through the formation of $\rho_{ee'}^{(2)}$. The third interaction produces the third-order electronic coherence $\rho_{eg}^{(3)}$ or $\rho_{eg}^{(3)}$ that gives rise to the signal according to equations (1) and (2). For more details on the use of DSFD, the reader is referred to [25–27, 43, 57].

The corresponding ladder diagrams [58] are also shown (see figure 2(b)). Each energy level is designated by a horizontal line with the time evolving from left to right. Interactions on the ket side are shown as solid vertical arrows and on the bra side as broken vertical arrows. For FWM processes such as CARS involving laser pulses with

a) Double-Sided Feynman Diagrams



b) Ladder Diagrams

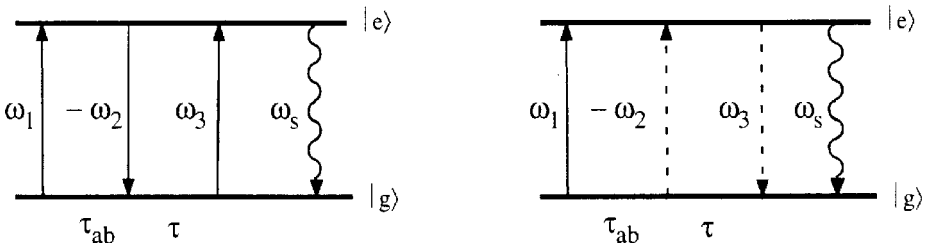


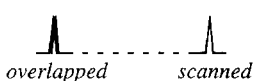
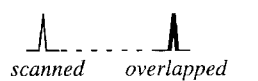
Figure 2. Diagrammatic representation of the processes that contribute to the VE signal when the time interval between the first two pulses is fixed. (a) The DSFDs show explicitly the time evolution of the density matrix when the fields act on the bra (right) or ket (left) side of the diagram and the time increases from bottom to top. The primed indices of these diagrams indicate different vibrational levels of the ground and excited electronic states. The diagram on the left, R_4 , is responsible for the observation of the ground-state dynamics. The diagram on the right, R_1 , is responsible for the excited-state dynamics. (b) The corresponding ladder diagrams illustrate explicitly the energy levels involved in each electronic interaction. A vertical broken or solid line represents interaction on the bra or the ket respectively. In these diagrams, time evolves from left to right.

different carrier frequencies, the ladder diagrams may be preferred because they depict energy explicitly [58]. Unfortunately, in this case it is not as easy to keep track of the state of the bra and ket after each pulse interaction as it is in the DSFD.

3. Experimental details

The experimental set-up used here has been described earlier [42, 46]. The experiments were performed with a home-built amplified colliding pulse mode-locked dye laser producing 60 fs pulses (transform-limited) centred around 620 nm. The bandwidth at full-width at half-maximum is typically about 8 nm. At the output of the laser amplifier, the femtosecond pulses were compensated for linear chirp in a double-pass prism arrangement with an average energy of 350 μJ . After the compression, the beam was split by two successive beam splitters into three beams of approximately equal intensity attenuated down to about 20 μJ each. The three beams were combined

Table 1. Summary of the observed phenomena for the different pulse sequences possible with the three laser pulses when two pulses overlap in time. For the experimental arrangement used here, there are only four distinguishable sequences (shown in bold type). Because beams E_a and E_c are equivalent, two additional (although not unique) sequences are possible. Sequences for which experimental data are presented have been labelled with an asterisk. The phenomena include TG, reverse-transient grating (RTG), reverse photon echo (RPE) and PE.

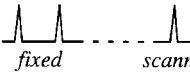
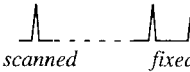
(I)		Sequences	(II)		
 overlapped scanned			 scanned overlapped		
<i>a b, c *</i> <i>c b, a</i>	$k_1 - k_1' + k_2$	Transient Grating	<i>a, b c</i> <i>c, b a *</i>	$k_1 - k_2 + k_2'$	Reverse TG
<i>a c, b *</i>	$k_1 + k_1' - k_2$	Reverse PE	<i>b, a c *</i>	$-k_1 + k_2' + k_2$	Photon Echo

in the usual FWM forward-box geometry and focused by a 500 mm lens in a quartz cell containing the iodine vapour (I_2). The amount of iodine in the cell was limited so that the optical density reaches a maximum of 0.4 and is independent of temperature for $T > 80$ °C. The experiments presented here were carried out at 140 °C. Pulses in one of the beams (E_c or E_b , depending on the set-up) were delayed with respect to the other two by a computer-controlled actuator (variable τ delay), while the fixed delay (τ_{nm} , where $n, m = a, b$ or c) was adjusted by delaying the pulses from the second beam with respect to the fixed one (beam E_a in all cases) using a micrometer.

All the experimental data were obtained in the direction $k_s = k_a - k_b + k_c$. The subindices a, b , and c can take any time order 1, 2 or 3; therefore, for the same phase-matching geometry, different phenomena such as PE or VE can be detected. The spatially filtered three-pulse FWM signal was collected by a spectrometer with a wide spectral acceptance (8 nm resolution). The transients were taken at 300–400 different time delays (about 200 shown) and averaged for nine scans. At each time delay τ , the signal was collected for ten laser shots. The laser intensity was monitored on a shot-to-shot basis; laser pulses with intensity outside one standard deviation were rejected. The accumulated laser intensity for each given time delay was stored and the final transients were normalized by this intensity. An effort was made to maintain similar laser intensities for all the transients and to present all transients using a consistent intensity scale to allow direct comparisons.

Three laser pulses can be arranged into six sequences ($abc, acb, bca, bac, cab, cba$), each having a distinct pulse ordering. For each pulse sequence, we can define time delays between the first and second pulse (τ_{12}) and the second and third pulses (τ_{23}) (see figure 1). We can divide the pulse sequences into those where two pulses overlap in time (table 1) and those where the three pulses are separated (table 2). We can further subdivide the pulse sequences into those where the first time delay is fixed (pulse sequence I (PS I)) and those for which the second time delay is fixed (pulse sequence II (PS II)). In the experiments presented here, the phase-matching geometry of detection (see figure 1(a)) makes fields E_a and E_c equivalent. The total number of unique combinations and permutations is ten; these are shown in bold type, being four in table 1 and six in table 2. The ten combinations lead to the observation of different nonlinear optical phenomena. Among them are TG, RTG (see table 1), VE, PE and C-FID-FWM (see table 2).

Table 2. Summary of the observed phenomena and the different pulse sequences possible with the three time-separated laser pulses. For the experimental arrangement used here, there are only six distinguishable sequences (shown in bold type). Because beams E_a and E_c are equivalent, additional (although not unique) sequences are possible. Sequences for which experimental data are presented have been labelled with an asterisk. The phenomena include VE, stimulated PE, and C-FID-FWM.

Phenomena	(I) Sequences	(II) Sequences
		
Virtual Photon Echo $\mathbf{k}_1 - \mathbf{k}_2 + \mathbf{k}_3$	$\mathbf{a} \mathbf{b}, \mathbf{c} *$ $\mathbf{c} \mathbf{b}, \mathbf{a}$ (VE I)	$\mathbf{a}, \mathbf{b} \mathbf{c}$ $\mathbf{c}, \mathbf{b} \mathbf{a} *$ (VE II)
Stimulated Photon Echo $-\mathbf{k}_1 + \mathbf{k}_2 + \mathbf{k}_3$	$\mathbf{b} \mathbf{a}, \mathbf{c} *$ $\mathbf{b} \mathbf{c}, \mathbf{a}$ (PE I)	$\mathbf{b}, \mathbf{a} \mathbf{c} *$ $\mathbf{b}, \mathbf{c} \mathbf{a}$ (PE II)
C-FID-FWM $\mathbf{k}_1 + \mathbf{k}_2 - \mathbf{k}_3$	$\mathbf{a} \mathbf{c}, \mathbf{b} *$ $\mathbf{c} \mathbf{a}, \mathbf{b}$ (C-FID-FWM I)	$\mathbf{a}, \mathbf{c} \mathbf{b}$ $\mathbf{c}, \mathbf{a} \mathbf{b} *$ (C-FID-FWM II)

The experimental data are shown together with the schematic diagrams of the pulse sequence and the applicable DSFDs. Many of the labels for the DSFDs have been omitted in order to simplify the diagrams here. The DSFDs corresponding to the formation of an excited state population after the first two interactions are shown on the right-hand side while the left-hand side diagrams correspond to formation of a ground-state population after the first two interactions. The time at which each field interacts with the system is indicated by a broken line. For the DSFDs shown in figures 3–8, the distance between these broken lines indicates the time delay, that is the smaller distance depicts the fixed time delay τ_{nm} and the larger distance depicts the variable time delay τ . When the fixed time delay is zero, only the variable time delay is reflected by the broken lines. The experimental transients show the FWM signal as a function of variable time delay τ . All FWM signals are displayed relative to each other, that is, the transients have not been rescaled. This allows for direct comparisons of signal intensity between the different pulse sequences.

4. Results and discussion

4.1. Overlapped pulses

Figure 3 displays the dynamics observed when two of the laser pulses are overlapped in time while the third pulse precedes or follows the other two. In the TG measurement (figure 3(a)), fields E_a and E_b are overlapped in time ($\tau_{ab} = 0$ fs) and field E_c follows at a variable time delay τ . Three DSFDs describe this process and indicate that both ground- and excited-state dynamics ($\rho_{g_g}^{(2)}$ and $\rho_{e_e}^{(2)}$ respectively) should be observed. In the first 2 ps of the transient, the 307 fs oscillations dominate, demonstrating the vibrational period of the B excited state of iodine. The transient also clearly shows 160 fs oscillations, reflecting the ground-state vibrational period of I_2 . Ground-state dynamics are more clearly observed at longer time delays because of wave packet spreading in the more anharmonic B excited state. We have taken the fast Fourier transform (FFT) of this transient [43, 44] and confirmed the assignment of the dynamics to the X- and B-state vibrations ($\nu' = 2-4$ and $\nu' = 6-11$).

In the RTG experiment [42] (figure 3(b)), the field E_c precedes the overlapped fields E_a and E_b . In this case, E_c excites an electronic coherence with a relaxation lifetime of

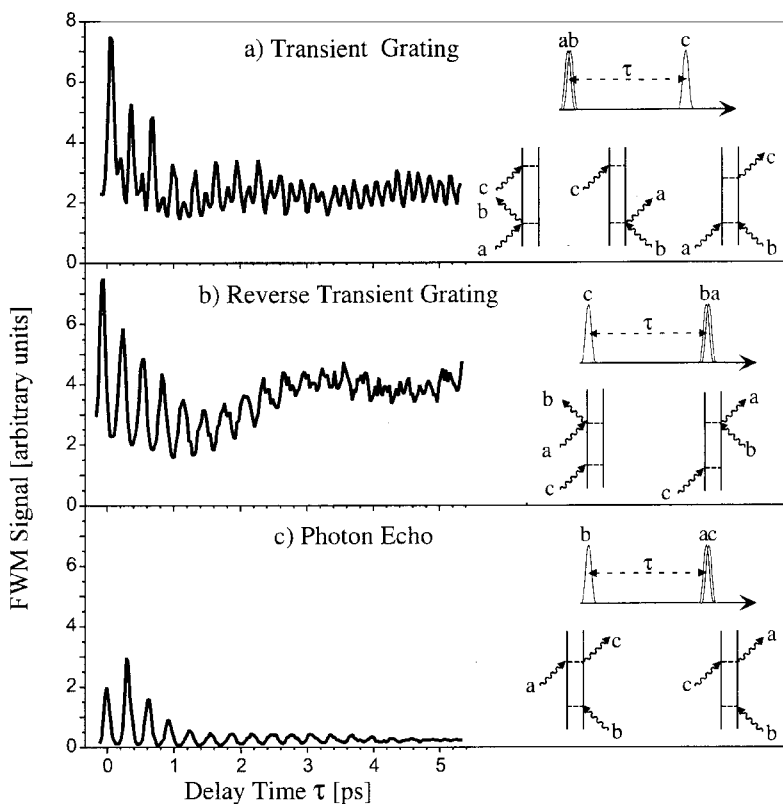


Figure 3. Experimental FWM data obtained for three different sequences having two pulses overlapped in time. The signal corresponds to three different phenomena: TG, RTG and PE, depending on the temporal arrangement of the electric fields. The pulse sequence and the DSFDs of the processes contributing to each phenomenon are included in each case. All plots are shown on the same scale in order to allow direct comparisons of the signal intensity. The dominant oscillation period in all cases, 307 fs, corresponds to excited-state vibrations. The transients from the TG and the RTG experiments in (a) and (b) show some additional contribution of ground-state vibrations. The transient from the RTG experiment presents a prominent slow modulation (2 ps) corresponding to rotational dephasing and a large background signal. Note that the PE data have a very small background and show only excited-state vibrations with very little rotational dephasing.

about 150 ps [64]. When E_b and E_c arrive, the grating is formed with E_b and the polarization generated by E_a . The observed vibrational dynamics are dominated by 307 fs oscillations, corresponding to the excited state of I_2 . A FFT of the transient confirms that the contribution of the excited state is greater than that of the ground state [43]. The time evolution of the coherence leads to the observation of both ground- and excited-state dynamics for this pulse sequence.

In the PE measurement (figure 3(c)), the pulse sequence is similar to that responsible for the RTG except that field E_b is applied first followed by E_a and E_c which are overlapped in time. The data show primarily excited-state dynamics, as can be observed in the transient. The most important difference between these transients is that field E_b acts first and is then followed by fields E_a and E_c . PE processes involve a rephasing of the coherence that is lost owing to inhomogeneities in the sample [27]. A direct comparison between the RTG and PE transients reveals that the slow

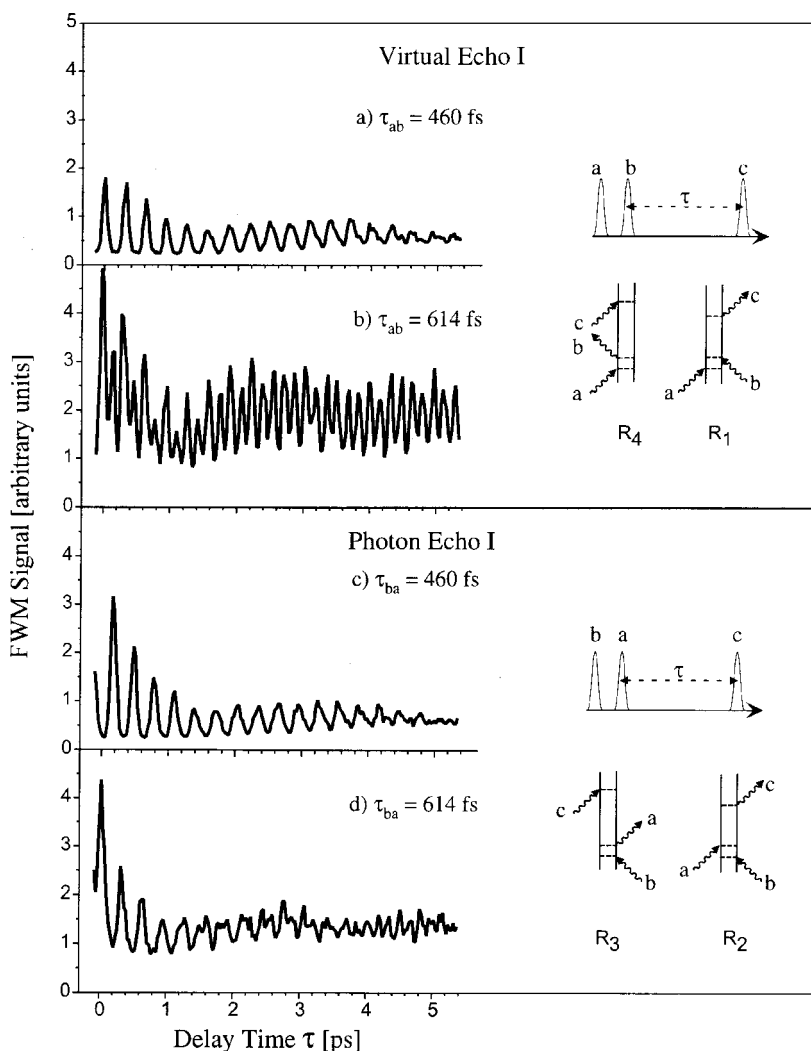


Figure 4. Experimental transients for sequences with fixed time delay between the first two pulses, PS I, with $\tau_{ab} = \tau_{ba} = 460$ and 614 fs. The VE I signal is obtained when the initial electric field acts on the ket side of the diagram and a PEI signal is obtained if the initial electric field acts on the bra side of the diagram. (a) When $\tau_{ab} = 460$ fs, the oscillation period of the VE signal corresponds to the vibrational motion of the excited-state molecules. (b) When $\tau_{ab} = 614$ fs, the VE signal oscillates with the ground-state vibrational frequency and the rotational dynamics (slow 2 ps modulation) are clearly observed. Note that the PE signals in (c) and (d) do not show the selectivity of the vibrational molecular motion based on the time delay τ_{ba} ; 307 fs oscillations corresponding to the excited state are the predominant feature in both transients.

undulation (2 ps) in the RTG measurement as well as the background are smaller in the PE transient. This difference is also apparent in the FFT of the PE and the RTG transients; the rotational contribution (peaks at frequencies less than 20 cm^{-1}) in the PE FFT are greatly reduced.

The predominance of the excited-state dynamics in both RTG and PE transients can be attributed to the fact that the wave packet motion in the excited state has a

much wider range of internuclear distances. This takes the wave packet in and out of the Franck–Condon region. Therefore, the electronic polarization reflects predominantly excited-state dynamics. Only in pulse sequences where pathways involving excited-state population transfer can be avoided, do the ground-state dynamics predominate. This selectivity in the observation of ground-state dynamics can be achieved by choosing a convenient time delay between the pulses, *vide infra*.

4.2. Pulse sequence I: virtual photon echo and stimulated photon echo

In figure 4, we use PS I (fixed delay followed by variable delay) to observe the dynamics obtained as the fixed delay is changed from 460 to 614 fs for virtual photon echo I (VE I) and stimulated photon echo I (PE I) sequences. In both cases, fields E_a and E_b are separated by a fixed time delay (τ_{ab} or τ_{ba}) and are followed by field E_c after a variable time delay τ . There are two DSFDs that apply to each of these pulse sequences; one shows $\rho_{g'g}^{(2)}$ and the other $\rho_{e'e}^{(2)}$. In the VE I measurement, when τ_{ab} is 460 fs (figure 4(a)) ($\frac{3}{2}\tau_e$ where $\tau_e = 2\pi/\omega_e$ for I_2 in the B state), the dynamics show 307 fs oscillations, reflecting only an excited-state contribution [43, 44]. When τ_{ab} is 614 fs (figure 4(b)) (twice the vibrational period of I_2 in the B state), the dynamics show 160 fs oscillations, reflecting predominately a ground-state contribution [43–46]. By changing the fixed time delay between fields E_a and E_b , the observation of excited- or ground-state dynamics of I_2 can be controlled. This coherent control should not be confused with control experiments without phase locking or phase matching [65].

In the PE I configuration, when τ_{ba} is 460 fs, the dynamics reflect an excited-state contribution with 307 fs oscillations; no ground-state contribution is observed in this transient. When τ_{ba} is 614 fs, the 307 fs oscillations still dominate; however, 2 ps later, 160 fs oscillations can be seen. Fourier transforms of these two PE transients confirm that, for $\tau_{ba} = 614$ fs, there is some ground-state contribution. The signal contribution due to rotational dynamics (slow 2 ps modulation) that is clearly observed in the VE I transients is much smaller in the PE I transients. Note that the selection between ground- or excited-state dynamics is much more efficient for the virtual echo set-up (figures 4(a) and (b)). The reason for this observation can be deduced from inspecting the DSFDs. For VE I, the DSFD that leads to the observation of ground state has three laser interactions acting on the ket. This leads to high selectivity between the two states. For VE I, the appearance of ground-state dynamics arises from a wave packet being prepared in the excited state, then pumped to the ground state and finally probed as a function of time, thereby giving a clear and intense ground-state signal. For PE I, the DSFD that leads to ground-state dynamics shows that the first two interactions are on the bra while the third interaction is on the ket. This action on an unperturbed ground state by the third pulse leads to loss of the selectivity. The reason for the small ground-state modulation in the PE I data is due to the interference between wave packets generated from different initial states, the equivalent of ‘hot bands’ in frequency-resolved spectroscopy.

In figure 5 (top), enlargements of the VE I and PE I transients for $\tau_{ab} = \tau_{ba} = 460$ fs are shown. It is clear that the two transients are exactly out of phase with each other; when one is at a maximum, the other is at a minimum. The applicable Feynman diagram for the observation of excited-state dynamics is on the right-hand side in each case of figure 4. In both cases, field E_c must interact with the wave packet formed in the excited state by field E_b . This process is depicted by action of E_c on the bra for both DSFDs responsible for excited-state populations. In figure 5 (bottom) schematic diagrams based on calculated wave packets of the excitation process after the first

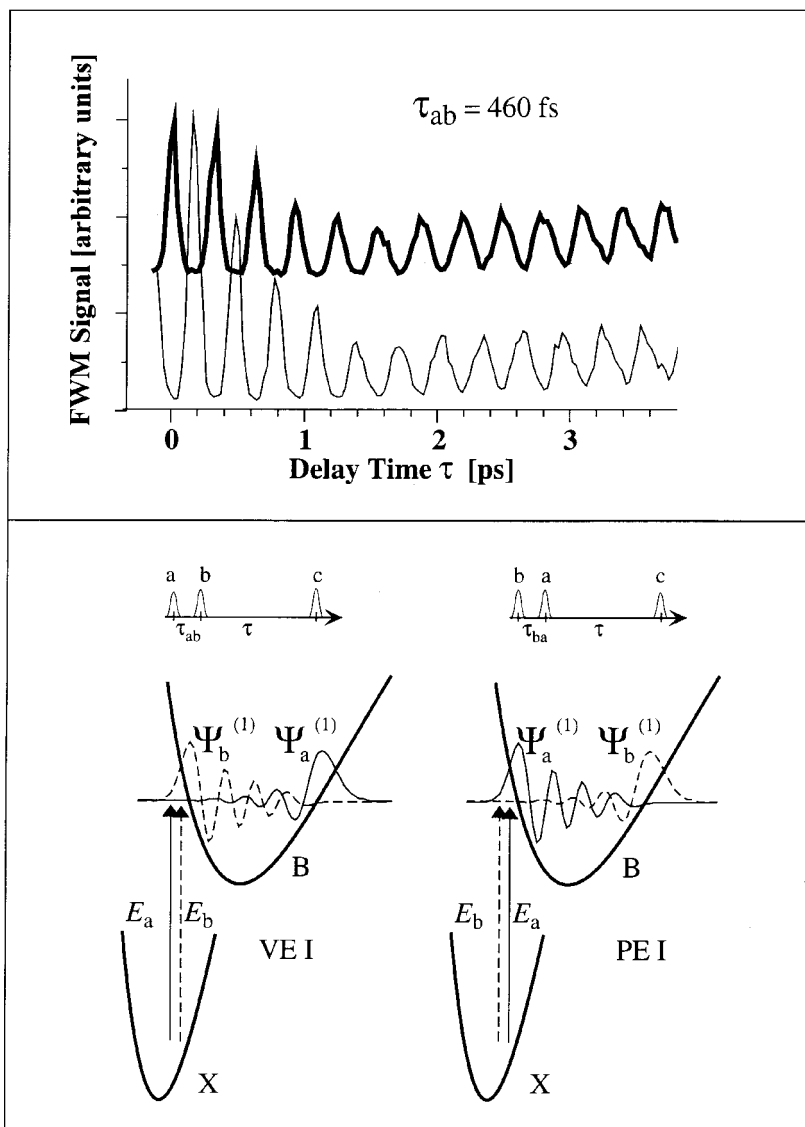


Figure 5. (Top) Experimental data for VE (—) and PE (---) measurements with $\tau_{ab} = \tau_{ba} = 460$ fs. Note that the signals, corresponding to excited-state dynamics, are exactly out of phase. The signal intensity has not been rescaled, but the VE I signal has been shifted vertically. Note that the PE signal peaks at 154 fs. The 180° phase difference between these transients can be understood by looking at the dynamics of the wave packet in the B state of I_2 resulting from the interaction with pulse E_b . (Bottom) Simulation of the wave packet motion on the B state of I_2 under the conditions of the VE I and PE I signals for PS I when $\tau_{ab} = \tau_{ba} = 460$ fs. In both cases, signal formation depends on de-excitation of $\Psi_b^{(1)}$ (---). At time delay $\tau = 0$ fs, which corresponds to the time delay between the second and third pulses, $\Psi_b^{(1)}$ is in the Franck–Condon region for VE I, maximizing the transition probability when the third pulse is applied there. However, for the PE I case, $\Psi_b^{(1)}$ is at the outer turning point of the excited-state potential when $\tau = 0$ fs, minimizing the transition probability when the third pulse is applied in the Franck–Condon region. In the PE I case, a delay of half a vibrational period is required to achieve the maximum observation of signal when the wave packet returns to the inner turning point.

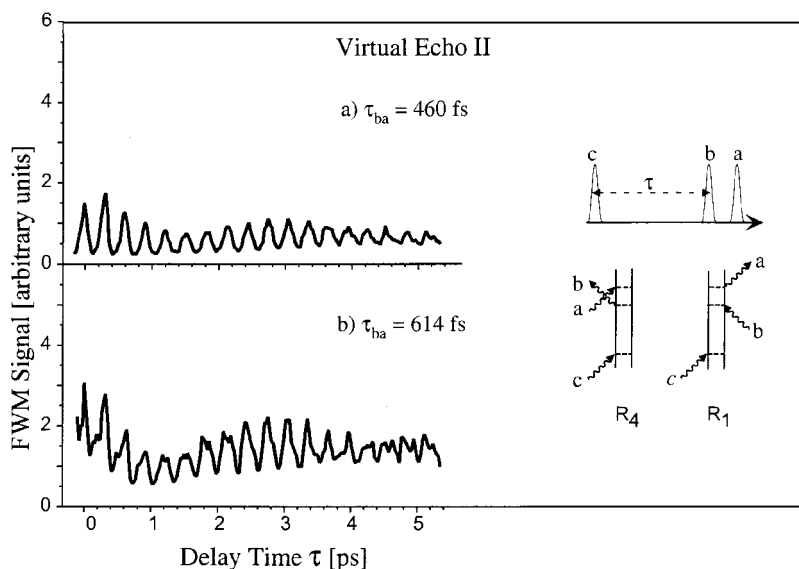


Figure 6. VE II transients obtained for a sequence having the time delay between the last two pulses fixed at $\tau_{ba} = 460$ and 614 fs. The vibrational excited-state motion dominates both transients. A very small contribution from the ground-state vibrational motion is apparent when $\tau_{ba} = 614$ fs. A larger rotational dephasing is observed (slow 2 ps modulation) in the $\tau_{ba} = 614$ fs signal and the signal intensity is higher in this case. The DSFDs of the processes that contribute to the signal are included together with the pulse sequence.

two electric fields are shown.[†] The wave packet resulting from excitation by field E_a is shown as a solid curve; the wave packet resulting from excitation by field E_b is shown as a broken curve. It is important to note that signal formation for both processes requires the de-excitation of the wave packet $\Psi_b^{(1)}$ by field E_c . In the VE case, field E_b interacts with the system secondly with $\tau_{ab} = 460$ fs. At $\tau = 0$ fs (time delay for field E_c with respect to the second pulse), the broken wave packet is at the inner turning point of the potential where the transition probability is maximized. Therefore the interaction results in a maximum signal. However, in the PE, field E_b interacts first with the system (still with $\tau_{ba} = 460$ fs). At $\tau = 0$ fs, the wave packet is at the outer turning point of the potential with negligible transition probability upon interaction with field E_c . After half a vibrational period, the wave packet returns to the inner turning point where the transition probability is maximized and the interaction with E_c produces a maximum signal. Therefore, the signals for PE I and VE I are exactly out of phase.

4.3. Pulse sequence II: virtual photon echo and stimulated photon echo

In figure 6, we examine PS II (variable time delay followed by fixed time delay) to observe the dynamics obtained as the fixed delay is changed from 460 to 614 fs. In this case, an electronic coherence is created by the first field E_c which evolves until fields E_b and E_a arrive. The fixed time delay can act as a ‘filter’ rather than a control parameter in selecting the observation of ground- or excited-state dynamics [43]. There are two applicable DSFDs for this configuration. The diagram on the left has all the

[†] We justify the use of wave packets to simulate the vibronic coherences because in the perturbation limit the ground state remains unchanged.

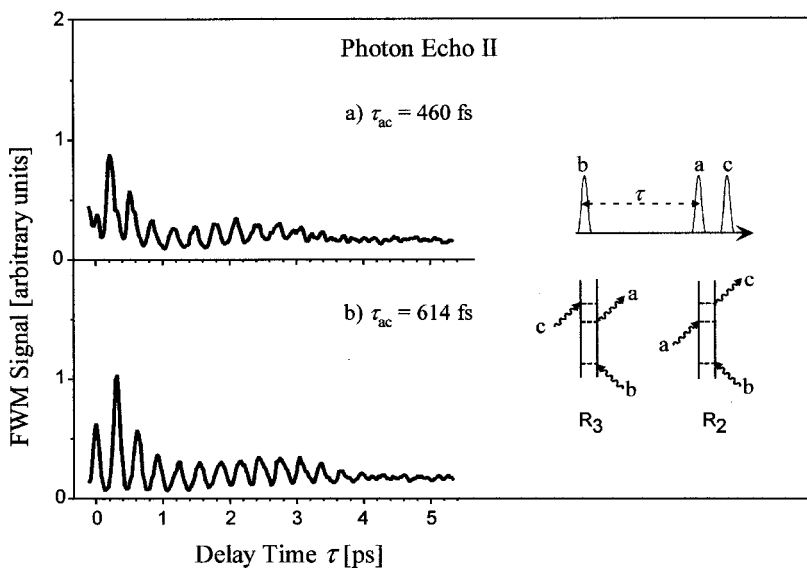


Figure 7. PE II transients obtained for PS II when $\tau_{ac} = 460$ and 614 fs. These transients, mostly dominated by the excited-state motion, do not show the selectivity of the molecular dynamics with the selection of the fixed time delay. In addition to the pulse sequence, the DSFDs of the processes that contribute to the signal are included.

interactions on the ket while the diagram on the right has the last two interactions on the bra. For $\tau_{ba} = 460$ fs, the transient shows 307 fs oscillations, corresponding to excited-state dynamics. The signal is weaker and shows only a small background. When $\tau_{ba} = 614$ fs, the transient is dominated by 307 fs oscillations. The signal is stronger and shows a larger background. Weak 160 fs vibrations are also observed. Fourier transforms have confirmed that the $\tau_{ba} = 614$ fs transient shows a contribution of the ground state [43]. For a time delay of $\tau_{ba} = 614$ fs, the observed background arises from the process depicted by the DSFD on the right. The use of the fixed delay as a filter for the dynamics changes the ground-state contributions to the signal slightly but does not give the same degree of control as is observed in the VE I case (see figures 4(a) and (b)).

In figure 7, we use PS II to observe the dynamics obtained as the fixed delay is changed 460 to 614 fs. In these measurements, field E_b precedes fields E_a and E_c , setting up a stimulated PE. The coherence generated by the first laser pulse is probed by the second and third pulses. The rotational dynamics, as evidenced by the slow 2 ps modulation, are significantly reduced in the PE II transients compared with those observed in the VE II transients. The transient in figure 7(a) shows predominately 307 fs dynamics and a small ground-state contribution. The transient shown in figure 7(b) reveals predominately excited-state contribution to the signal. These assignments were confirmed by FFT.

4.4. Free-induction decay and four-wave mixing

So far we have discussed a number of phenomena and outlined the rules for their diagrammatic representation. The identification of the eight different diagrams that can contribute to the signal under the RWA has been shown in a number of publications [25, 27]. When a particular sequence of resonant fields violates the RWA, the FWM signal should not be observed (is negligible). An example would be the

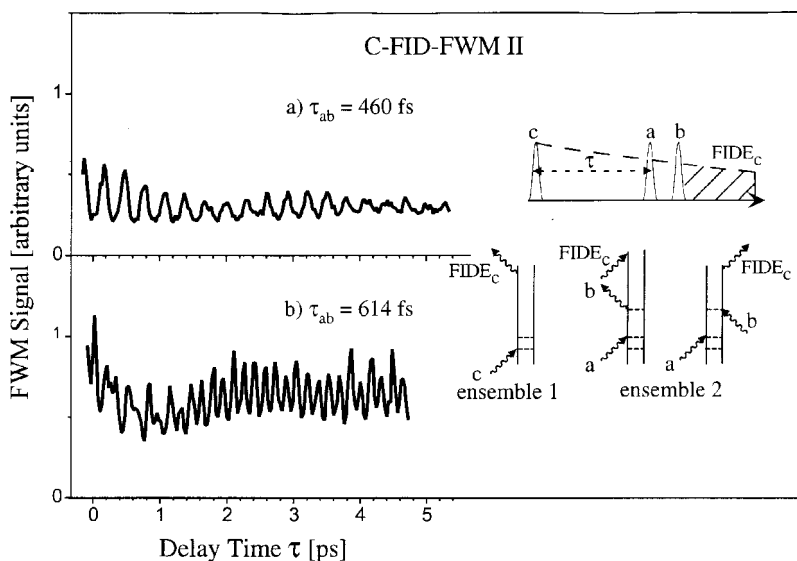


Figure 8. C-FID-FWM II transients for PS II for $\tau_{ab} = 460$ and 614 fs. When $\tau_{ab} = 460$ fs, the oscillation period of the C-FID-FWM signal corresponds to the vibrational motion of the excited-state molecules, whereas when $\tau_{ab} = 614$ fs the signal oscillates with the ground-state vibrational frequency and shows a larger rotational modulation (2 ps). Note that the data are very similar to those observed for VE I (figure 4(a) and (b)). This implies that the dominant pathway for signal formation can be illustrated using similar DSFDs for the two ensembles: one to indicate the stimulation of the FIDE from beam E_c , FIDE_c , and the other to indicate the formation of the C-FID-FWM II signal, represented as a shaded area in the pulse sequence plot.

sequence $\mathbf{k}_1 + \mathbf{k}_2 - \mathbf{k}_3$ for a two-electronic-states system. This corresponds to pulses E_a and E_c preceding pulse E_b . We set out to test this hypothesis and detected weak signals corresponding to an interesting FWM phenomena that arises under certain conditions described below.

In figure 8, we present the signal obtained with the pulse sequence E_c followed by E_a and E_b . The signal intensity is a factor of about four lower than the VE I data. It is remarkable to see that, when $\tau_{ab} = 460$ fs, the transient shows 307 fs oscillations, corresponding to excited-state dynamics. When $\tau_{ab} = 614$ fs, 160 fs oscillations are evident, indicating ground-state dynamics. Therefore, we are able to observe ground- or excited-state dynamics by changing the fixed time delay as was done in VE I (see figures 4(a) and (b)). Our explanation for this process is that the field E_c creates a first-order polarization that decays by FIDE with time $T_2 > 50$ ps [64]. This emission is designated as FIDE_c . Beams E_a and E_b form the grating with populations $\rho_{gg}^{(2)}$ and $\rho_{ee}^{(2)}$; then the FIDE_c Bragg diffracts from the grating to form the signal. Because the FIDE is generated in a separate ensemble of molecules we designate this process a cascade—hence the abbreviation C-FID-FWM. This situation is similar to the VE I measurements except that the beam E_c is replaced by FIDE_c . The observation of selectivity between ground- and excited-state dynamics confirms the interpretation of this phenomenon. Note that the only way to represent this first-order cascading process diagrammatically is by invoking two ensembles: one responsible for the first-order polarization and the other for the FWM process. This explanation does not involve a violation of the RWA.

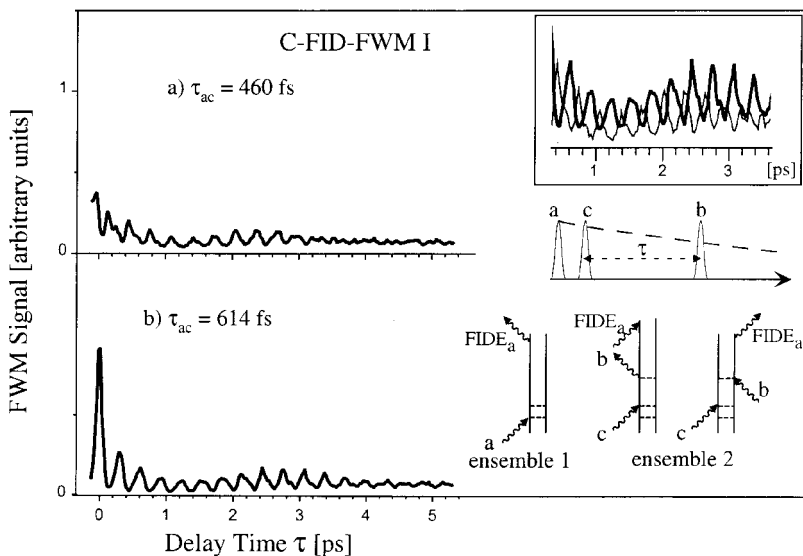


Figure 9. C-FID-FWM I transients for PS I for $\tau_{ac} = 460$ and 614 fs. Note that the signal intensity for these sequences is quite low, especially after the first picosecond. The transients do not show selectivity between the ground- and excited-state molecular dynamics with the fixed time delay. However, the change in the time delay causes a shift in the phase of the observed vibrational oscillations. In the insets, the thin curve depicts the experimental data when the fixed time delay is 460 fs, and the thick curve shows the oscillations when the fixed time delay is 614 fs. The out-of-phase behaviour can be seen in these plots. The pulse sequence and the coupled DSFD are included for each case.

The signal identified here as C-FID-FWM arises when the sample has a relatively long-lived polarization, the lasers are resonant with a transition and the sample is in a relative high concentration. Under these conditions each pulse generates a FID with an integrated emission intensity that can be comparable with the field that induces it. The FIDE under these circumstances participates in the formation of FWM signal. This type of signal is best observed when other FWM processes are forbidden. Observation of this type of signal can be found in the work of Kinrot and Prior [66]. The effect is related to the Lorentz local-field correction to nonlinear optical processes introduced by Bloembergen [67] (see also [26]).

PS I is used to explore other C-FID-FWM signals shown in figure 9. For both transients in this figure, $\tau_{ac} = 460$ fs and $\tau_{ac} = 614$ fs, the dynamics are dominated by excited-state vibrations. FFT confirms this observation. The ground-state contribution is slightly higher for the transient with $\tau_{ac} = 614$ fs than for $\tau_{ac} = 460$ fs. These transients can be interpreted as follows. Fields E_c and E_b form the grating; then the FIDE stimulated by E_a , denoted FIDE_a, mixes to form the signal, C-FID-FWM I. Because the fixed time delay is now between the first two pulses, one participating in the population formation and the second in the generation of FIDE_a, selectivity is not expected between ground- and excited-state dynamics. The time delay difference between the first two pulses is half the excited-state vibrational period. This causes the $\tau_{ac} = 460$ fs transient to be similar to the $\tau_{ac} = 614$ fs transient except for being out of phase by half a vibrational period (154 fs). This change in phase can be seen in the insets in figure 9 where the thin curve represents $\tau_{ac} = 460$ fs and the thick curve shows the $\tau_{ac} = 614$ fs data.

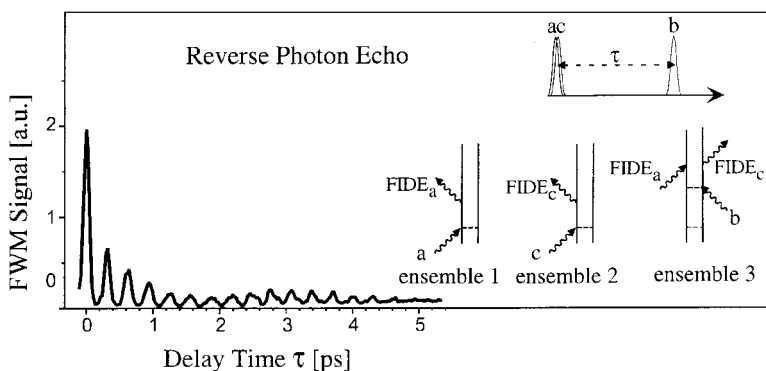


Figure 10. RPE transients when the first two pulses are overlapped in time (a.u., arbitrary units). The signal intensity for these sequences is relatively low, especially after the first picosecond. The pulse sequence and the coupled DSFD are included. Note that the data have a very small background and show only excited-state vibrations.

The signal obtained when fields E_a and E_c are overlapped in time and are followed by field E_b is shown in figure 10. The signal intensity is a factor of about four smaller than the comparable PE signal shown in figure 3(c). Although this pulse sequence does not satisfy the RWA and should not produce a signal in the phase-matching direction, we did obtain signal with 307 fs vibrations as seen in the transient. The data can be explained using a similar argument as for the other C-FID-FWM processes. Pulses E_a and E_c induce a first-order polarization each with FIDE_a and FIDE_c . These two fields mix with beam E_b to form a cascaded FWM signal involving three molecular ensembles. Note that this pulse sequence is the time reversal of the PE pulse sequence in figure 3(c) and the DSFD diagram corresponding to the C-FID-FWM signal is similar to that in figure 3(c) for PE data. The signals in both cases are very similar except for the difference in intensities. For these reasons we can justify the use of the term reverse photon echo (RPE) [68].

5. Conclusions

In this article we compare the different phenomena that can be observed with femtosecond pulses on gas-phase molecules for different pulse sequences. Here we have shown that three laser pulses can generate six different nonlinear optical phenomena: virtual echo, photon echo, transient grating, reverse-transient grating C-FID-FWM and reverse photon echo. While these phenomena are closely related, it is important to distinguish between them. Some allow the experimenter to control the observation of ground- or excited-state dynamics. Others allow the control of the phase of the observed molecular vibrations. Finally, some of these techniques achieve cancellation or enhancement of inhomogeneous broadening.

One of the important conclusions of this article is the distinction between the bra and ket laser interactions. Quantum-mechanically, the transition probability from state g to state e depends on $\langle e|\mu E|g\rangle\langle g|\mu E|e\rangle^*$, implying a double interaction. The physical basis for the double interaction comes from the fact that the electric field has two components $\exp[i(\mathbf{k}\cdot\mathbf{r}-\omega t)]$ and $\exp[-i(\mathbf{k}\cdot\mathbf{r}-\omega t)]$. Molecules may interact with either of the components (thus forming a coherence state) or with both (thus forming a population in the original or in the new state). Starting from the ground state and invoking the rotating wave approximation, a ket interaction can only be achieved with $\exp[i(\mathbf{k}\cdot\mathbf{r}-\omega t)]$ and a bra interaction can only be achieved with $\exp[-i(\mathbf{k}\cdot\mathbf{r}-\omega t)]$.

When the three incident pulses have distinguishable wave-vectors, as for most non-collinear geometries, one is able to define a phase-matching geometry that determines the sign and hence the nature of each electric field interaction. Therefore, a distinction between a bra or a ket interaction can be experimentally achieved.

The distinction that arises from the geometric arrangement of the lasers and the possibility to have fixed or variable time delay between them leads to the ten unique pulse sequences described in tables 1 and 2. The data presented show several differences. For stimulated PE measurements, the signal does not contain elements that can be attributed to inhomogeneous broadening while VE measurements do. This difference is best shown in figure 3 by comparing the RTG (see figure 3(b)) and the PE signals (see figure 3(c)). We have recently conducted coherence relaxation measurements on gas-phase iodine as a function of temperature. We found that the PE relaxation times were always longer than the corresponding VE relaxation times and were also temperature dependent, as expected. The relaxation measurements for RTG measurements were dominated by inhomogeneous contributions such as Doppler broadening and the Boltzmann distribution of states prior to laser excitation [64]. One of the strategies used here to sort different processes was to delay a pair of pulses by a fixed time interval, chosen to be equal to an integral or a half-integral number of vibrational oscillations of the excited state. This reveals a striking difference between VE and PE measurements as shown in figure 4 where the VE I signal shows excited- or ground-state dynamics depending on the delay between the first two pulses. However, we note that for PE measurements this control is not observed. The reason for this observation is that one of the diagrams for VE involves all three interactions on the ket. This places a restriction on the laser-molecule interactions, requiring that the electric field interactions must be in concert with the vibrational dynamics. The PE diagram that corresponds to the formation of a population in the ground state is not as restrictive because only the third pulse acts on the ket. From the viewpoint of control over ground- or excited-state dynamics, the sequence $\mathbf{k}_1 - \mathbf{k}_2 + \mathbf{k}_3$, labelled VE I, is the most efficient. This phenomenon is easily observed in gas-phase samples; however, in liquids, VE is usually not observed because of inhomogeneous broadening.

Our PE results agree with the well-known property of PE signals, namely that the effect of inhomogeneities is cancelled [2]. A technique aimed at suppressing excited-state dynamics was introduced in the 1990s by Shank and co-workers [69, 70]. The mode suppression technique requires fixing the time delay between the first and third pulses while the second pulse is scanned in the pulse sequence $\mathbf{k}_s = -\mathbf{k}_1 + \mathbf{k}_2 + \mathbf{k}_3$. The method has been found to work only in cases of extremely large inhomogeneous broadening [71, 72]. We have explored the mode suppression method under the same conditions as all the transients in this article. We found that the apparent suppression of excited-state coherent vibrations is achieved by a combination of Liouville pathways that allows ground- and excited-state contributions, thereby drowning the pure excited-state dynamics that are observed when the time delay between the first and third pulses are out of phase with the excited-state oscillations [64].

In this article, we explore the C-FID-FWM phenomenon in the gas phase. This signal is observed for pulse sequences where conventional diagrammatic techniques fail to predict the appearance of signal. The observed signal is not caused by a higher-order nonlinear process or from a breakdown of the RWA. As described earlier, the C-FID-FWM signal is caused by an induced polarization that maintains the phase and the vectorial characteristics of the pumping beam. Because the coherence

relaxation in iodine at this temperature has a lifetime of about 10^{-10} s, the FIDE can act at relatively long times. The participation of an electric field generated by a polarization in a nonlinear optical process has precedents; this phenomenon is called cascading [73, 74]. More recently, cascading has been implicated in the signal arising in fifth-order nonlinear processes. Upon close inspection the fifth-order signal has been found to result from two third-order processes that have been called sequential CARS or cascade [75–77]. The emission from one third-order polarization participates in a different third-order polarization [75–77].

The data being reported here show a different type of FWM cascading. The differences are as follows.

- (i) Resonance excitation leads to long-lived polarizations that can interact with the other laser pulses at very long times.
- (ii) In the studies from the Albrecht and Fleming groups, the cascading process is a combination of two third-order processes while, in our case, the C–FID–FWM signal results from a first-order process and a second-order process.
- (iii) In our measurements, we have used only three pulses instead of four or five.
- (iv) We have observed a C–FID–FWM in a gas-phase sample.

Thus, we have ensured that phase matching occurs only for the third-order process of interest and that the observation of FWM or C–FID–FWM depends on only on the pulse sequence.

The C–FID–FWM transients presented here show two surprising effects: the signal is measurable and the femtosecond time resolution is maintained. Given that at least one of the electric fields is replaced by the FIDE, one could conclude that the intensity would be much lower and that the time resolution would be lost because of the picosecond lifetime of that emission. The intensity of the C–FID–FWM signal derives from the integral over the long duration of the FIDE. In fact, we have found that in addition to the concentration dependence the ratio of C–FID–FWM to FWM depends on the ratio $T_2^2/(T_1 \tau_p)$, where T_2 is the coherence relaxation time, T_1 is the emission lifetime and τ_p is the laser pulse duration [78]. The temporal resolution is maintained because the FIDE arises from a vibronic coherence. Therefore, it is strongly coupled to the coherent vibrational motion in the ground and excited states, being modulated on the femtosecond time scale. A theoretical simulation of these data will be published elsewhere [78].

Coherent control of chemical reactions depends on the design of an electric field capable of causing a molecular system to yield a specified product. These special fields can be constructed out of coherently coupling multiple laser pulses. This work studies the coherent coupling of three fields using the phase-matching condition and the third-order nonlinear response of the sample as filters of the incoherent contributions. The exploration of the various phenomena allows us to form a ‘toolkit’ that can be used to achieve the coherent control. Our understanding shows that with FWM the most efficient control is achieved when the phase-matching geometry and the pulse sequence lead to all laser interactions occurring on the ket. This implies using what we have called the VE I pulse sequence.

In conclusion, we have presented experimental data for ten different sequences stemming from three degenerate femtosecond laser pulses. Our data highlight the need for understanding that laser–molecule interactions take place on a complex frame that can be understood by interaction with $\exp[-i(\mathbf{k} \cdot \mathbf{r} - \omega t)]$ or with $\exp[i(\mathbf{k} \cdot \mathbf{r} - \omega t)]$. In

the language of quantum mechanics, these interactions correspond to the bra or the ket respectively for the first pulse. Based on this understanding, diagrams can be drawn to understand the nature of the measurement, whereas density matrix calculations can then be used to simulate the data. Sorting out all the different phenomena is valuable for understanding different nonlinear optical measurements from different groups. Finally, the observation of the C–FID–FWM transients is an example of nonlinear experiments where the pulses are at least one order of magnitude shorter than the coherence of the sample.

Acknowledgements

This research was partially funded by a grant from the National Science Foundation (CHE-9812584). M.D. is a Lucille and David Packard Science and Engineering Fellow, a Camille Dreyfus Teacher–Scholar and an Alfred P. Sloan Fellow, E.J.B. is supported by a National Science Foundation Graduate Fellowship. I.P. gratefully acknowledges a James L. Dye Endowment Fellowship.

References

- [1] KURNIT, N. A., ABELLA, I. D., and HARTMANN, S. R., 1964, *Phys. Rev. Lett.*, **13**, 567.
- [2] PATEL, C. K. N., and SLUSHER, R. E., 1968, *Phys. Rev. Lett.*, **20**, 1087.
- [3] LUKASIK, J., and DUCUING, J., 1972, *Phys. Rev. Lett.*, **28**, 1155.
- [4] HERITAGE, J. P., GUSTAFSON, T. K., and LIN, C. H., 1975, *Phys. Rev. Lett.*, **34**, 1299.
- [5] ABRAMS, R. L., LAM, J. F., LIND, R. C., STEEL, D. G., and LIAO, P. F., 1983, *Optical Phase Conjugation*, edited by R. A. Fisher (San Diego, California: Academic Press) p. 211.
- [6] KENNEY-WALLACE, G. A., and WALLACE, S. C., 1983, *IEEE J. quant. Electron.*, **19**, 719.
- [7] ROSE, T. S., WILSON, W. L., WÄCKERLE, G., and FAYER, M. D., 1987, *J. chem. Phys.*, **86**, 5370.
- [8] LEVENSON, M. D., and KANO, S., 1988, *Introduction to Nonlinear Laser Spectroscopy* (Boston, Massachusetts: Academic Press).
- [9] FOURKAS, J. T., BREWER, T. R., KIM, H., and FAYER, M. D., 1991, *J. chem. Phys.*, **95**, 5775.
- [10] HESSELINK, W. H., and WIERSMA, D. A., 1979, *Phys. Rev. Lett.*, **43**, 1991.
- [11] EISENTHAL, K. (editor), 1984, *Applications of Picosecond Spectroscopy to Chemistry* (Dordrecht: Reidel).
- [12] FLEMING, G. R., 1986, *Chemical Applications of Ultrafast Spectroscopy* (Oxford University Press).
- [13] MYERS, A. B., and HOCHSTRASSER, R. M., 1986, *IEEE J. quant. Electron.*, **22**, 1482.
- [14] DUPPEN, K., and WIERSMA, D. A., 1986, *J. opt. Soc. Am. B*, **3**, 614.
- [15] WIERSMA, D. A., and DUPPEN, K., 1987, *Science*, **237**, 1147.
- [16] KASINSKI, J. J., GOMEZ-JAHN, L., GRACEWSKI, S. M., FARAN, K. J., and MILLER, R. J. D., 1989, *J. chem. Phys.*, **90**, 1253.
- [17] GENBERG, L., BAO, Q., GRACEWSKI, S., and MILLER, R. J. D., 1989, *Chem. Phys.*, **131**, 81.
- [18] YAN, Y.-X., CHENG, L.-T., and NELSON, K. A., 1987, *Advances in Non-Linear Spectroscopy*, edited by R. J. H. Clark and R. E. Hester (Chichester, West Sussex: Wiley) pp. 299–355.
- [19] CHESNOY, J., and MOKHTARI, A., 1988, *Phys. Rev. A*, **38**, 3566.
- [20] MCMORROW, D., LOTSHAW, W. T., and KENNEY-WALLACE, G. A., 1988, *IEEE J. quant. Electron.*, **24**, 443.
- [21] NIBBERING, E. T. J., WIERSMA, D. A., and DUPPEN, K., 1991, *Phys. Rev. Lett.*, **66**, 2464.
- [22] CHO, M., ROSENTHAL, S. J., SCHERER, N. F., ZIEGLER, L. D., and FLEMING, G. R., 1992, *J. chem. Phys.*, **96**, 5033.
- [23] SCHERER, N. F., ZIEGLER, L. D., and FLEMING, G. R., 1992, *J. chem. Phys.*, **96**, 5544.
- [24] DHAR, L., ROGERS, J. A., and NELSON, K. A., 1994, *Chem. Rev.*, **94**, 157.
- [25] SHEN, Y. R., 1984, *The Principle of Nonlinear Optics* (New York: Wiley).
- [26] BOYD, R. W., 1992, *Nonlinear Optics* (San Diego, California: Academic Press).
- [27] MUKAMEL, S., 1995, *Principles of Nonlinear Optical Spectroscopy* (Oxford University Press).

- [28] CLARK, R. J. H., and HESTER, R. E. (editors), 1987, *Advances in Non-Linear Spectroscopy*, Vol. 15 (Chichester, West Sussex: Wiley).
- [29] FAYER, M. D., 1982, *A. Rev. phys. Chem.*, **33**, 63.
- [30] ROSE, T. S., and FAYER, M. D., 1985, *Chem. Phys. Lett.*, **117**, 12.
- [31] MORGEN, M., PRICE, W., HUNZIKER, L., LUDOWISE, P., BLACKWELL, M., and CHEN, Y., 1993, *Chem. Phys. Lett.*, **209**, 1.
- [32] MORGEN, M., PRICE, W., LUDOWISE, P., and CHEN, Y., 1995, *J. chem. Phys.*, **102**, 8780.
- [33] HAYDEN, C. C., and CHANDLER, D. W., 1995, *J. chem. Phys.*, **103**, 10465.
- [34] MOTZKUS, M., PEDERSEN, S., and ZEWAIL, A. H., 1996, *J. phys. Chem.*, **100**, 5620.
- [35] SCHMITT, M., KNOPP, G., MATERNY, A., and KIEFER, W., 1997, *Chem. Phys. Lett.*, **270**, 9.
- [36] SCHMITT, M., KNOPP, G., MATERNY, A., and KIEFER, W., 1997, *Chem. Phys. Lett.*, **280**, 339.
- [37] MEYER, S., SCHMITT, M., MATERNY, A., KIEFER, W., and ENGEL, V., 1997, *Chem. Phys. Lett.*, **281**, 332.
- [38] CHEN, T., ENGEL, V., HEID, M., KIEFER, W., KNOPP, G., MATERNY, A., MEYER, S., PAUSCH, R., SCHMITT, M., SCHWOERER, H., and SIEBERT, T., 1999, *J. molec. Struct.*, **481**, 33.
- [39] MEYER, S., SCHMITT, M., MATERNY, A., KIEFER, W., and ENGEL, V., 1998, *Chem. Phys. Lett.*, **287**, 753.
- [40] FREY, H. M., BEAUD, P., GERBER, T., MISCHLER, B., RADI, P. P., and TZANNIS, A. P., 1999, *Appl. Phys. B*, **68**, 735.
- [41] KNOPP, G., PINKAS, I., and PRIOR, Y., 2000, *J. Raman Spectrosc.*, **31**, 51.
- [42] BROWN, E. J., ZHANG, Q., and DANTUS, M., 1999, *J. chem. Phys.*, **110**, 5772.
- [43] PASTIRK, I., BROWN, E. J., GRIMBERG, B. I., LOZOVY, V. V., and DANTUS, M., 1999, *Faraday Discuss.*, **113**, 401.
- [44] BROWN, E. J., PASTIRK, I., GRIMBERG, B. I., LOZOVY, V. V., and DANTUS, M., 1999, *J. chem. Phys.*, **111**, 3779.
- [45] PASTIRK, I., LOZOVY, V. V., GRIMBERG, B. I., BROWN, E. J., and DANTUS, M., 1999, *J. phys. Chem. A*, **103**, 10226.
- [46] LOZOVY, V. V., GRIMBERG, B. I., BROWN, E. J., PASTIRK, I., and DANTUS, M., 2000, *J. Raman Spectrosc.*, **31**, 41.
- [47] MULLIKEN, R. S., 1971, *J. chem. Phys.*, **55**, 288.
- [48] TELLINGHUISEN, J., 1978, *J. Quant. Spectrosc. Radiat. Transfer*, **19**, 149.
- [49] LOZOVY, V. V., TITOV, A. A., GOSTEV, F. E., TOVBIN, D. G., ANTIPIN, S. A., UMANSKII, S. Y., and SARKISOV, O. M., 1998, *Chem. Phys. Rep.*, **17**, 1267.
- [50] TANNOR, D. J., RICE, S. A., and WEBER, P. M., 1985, *J. chem. Phys.*, **83**, 6158.
- [51] MEYER, S., SCHMITT, M., MATERNY, A., KIEFER, W., and ENGEL, V., 1999, *Chem. Phys. Lett.*, **301**, 248.
- [52] GRIMBERG, B. I., LOZOVY, V. V., DANTUS, M., and MUKAMEL, S., 2000, *J. phys. Chem.* (submitted).
- [53] YEE, T. K., and GUSTAFSON, T. K., 1978, *Phys. Rev. A*, **8**, 1597.
- [54] BORDÉ, J., and BORDÉ, C. J., 1979, *J. molec. Spectrosc.*, **78**, 353.
- [55] PRIOR, Y., 1984, *IEEE J. quant. Electron.*, **20**, 37.
- [56] ROTHBERG, L. J., and BLOEMBERGEN, N., 1984, *Phys. Rev. A*, **30**, 820.
- [57] VACCARO, P. H., 1997, *Nonlinear Spectroscopy for Molecular Structure Determination*, edited by E. Hirota, R. W. Field, J. P. Maier and S. Tsuchiya (Oxford: Blackwell Scientific) pp. 75–126.
- [58] LEE, D., and ALBRECHT, A. C., 1985, *Advances in Infrared and Raman Spectroscopy*, Vol. 12, edited by R. J. H. Clark and R. E. Hester (Chichester, West Sussex: Wiley–Heyden) pp. 179–213.
- [59] PSHENICHNIKOV, M. S., DE BOEIJ, W. P., and WIERSMA, D. A., 1996, *Phys. Rev. Lett.*, **76**, 4701.
- [60] DE BOEIJ, W. P., PSHENICHNIKOV, M. S., and WIERSMA, D. A., 1998, *Chem. Phys.*, **233**, 287.
- [61] CHACHISVILIS, M., FIDDER, H., and SUNDSTRÖM, V., 1995, *Chem. Phys. Lett.*, **234**, 141.
- [62] KIRKWOOD, J. C., and ALBRECHT, A. C., 2000, *Phys. Rev. A*, **61**, 3802.
- [63] STEINFELD, J. I., 1978, *Laser and Coherence Spectroscopy* (New York: Plenum Press).
- [64] LOZOVY, V. V., BROWN, E. J., PASTIRK, I., GRIMBERG, B. I., and DANTUS, M., 2000, in *Coherent Control of Chemical Reaction Dynamics*, edited by R. J. Gordon and Y. Fujimura (Singapore: World Scientific) (in the press).
- [65] GERDY, J. J., DANTUS, M., BOWMAN, R. M., and ZEWAIL, A. H., 1990, *Chem. Phys. Lett.*, **171**, 1.

- [66] KINROT, O., and PRIOR, Y., 1994, *Phys. Rev. A*, **50**, 1999.
- [67] BLOEMBERGEN, N., 1965, *Nonlinear Optics* (New York: Benjamin).
- [68] ZHANG, W. M., CHERNYAK, V., and MUKAMEL, S., 1999, *J. chem. Phys.*, **110**, 5011.
- [69] BARDEEN, C. J., and SHANK, C. V., 1993, *Chem. Phys. Lett.*, **203**, 535.
- [70] SCHOENLEIN, R. W., MITTLEMAN, D. M., SHIANG, J. J., ALIVISATOS, A. P., and SHANK, C. V., 1993, *Phys. Rev. Lett.*, **70**, 1014.
- [71] DE BOEIJ, W. P., PSHENICHNIKOV, M. S., and WIERSMA, D. A., 1996, *J. chem. Phys.*, **105**, 2953.
- [72] DE BOEIJ, W. P., PSHENICHNIKOV, M. S., and WIERSMA, D. A., 1998, *Annu. Rev. phys. Chem.*, **49**, 99.
- [73] MEREDITH, G. R., 1982, *Phys. Rev. B*, **24**, 5522.
- [74] MEREDITH, G. R., 1982, *J. chem. Phys.*, **77**, 5863.
- [75] ULNESS, D. J., KIRKWOOD, J. C., and ALBRECHT, A. C., 1998, *J. chem. Phys.*, **108**, 3897.
- [76] KIRKWOOD, J. C., ULNESS, D. J., ALBRECHT, A. C., and STIMSON, M. J., 1998, *Chem. Phys. Lett.*, **293**, 417.
- [77] BLANK, D. A., KAUFMAN, L. J., and FLEMING, G. R., 1999, *J. chem. Phys.*, **111**, 3105.
- [78] LOZOVY, V. V., PASTIRK, I., and DANTUS, M., 2000, *Chem. Phys. Lett.*, (submitted).